Low Temperature Physics/Fizika Nizkikh Temperatur, 2021, vol. 47, No. 6, pp. 501–508

Two-dimensional Berezinskii–Kosterlitz–Thouless topological phase transition in three-dimensional $Bi_2Sr_2Ca_2Cu_3O_{10+x}$:(La,Sr)MnO_3 nanocomposites

A. I. D'yachenko

G. V. Kurdyumov Institute of Metal Physics of the National Academy of Sciences of Ukraine, Kyiv 03142, Ukraine

V. N. Krivoruchko and V. Yu. Tarenkov

O. O. Galkin Donetsk Institute for Physics and Engineering of the National Academy of Sciences of Ukraine
Kyiv 03028, Ukraine
E-mail: krivoruc@gmail.com

Received February 13, 2021, revised March 11, 2021, published online April 26, 2021

Electrical transport properties of random binary networks composed of high-T_c superconductor $Bi_2Sr_2Ca_2Cu_3O_{10+x}$ (Bi2223) microparticles and half-metal ferromagnet $La_{2/3}Sr_{1/3}MnO_3$ (LSMO) nanoparticles have been investigated. The experimental current-voltage characteristics of bulk samples of nanocomposites with a volumetric content of 4:1 components are well described by the Berezinsky–Kosterlitz–Thouless (BKT) model for two-dimensional (2D) superconductors undergoing a superconducting transition. The observed 2D-like behavior of the three-dimensional transport properties of the nanocomposite is most likely associated with two different physical spatial scales involved in the formation of the properties of the nanocomposite: a significant difference between the geometric dimensions of the constituent components and the appearance of a triplet superconducting state induced by the proximity effect in semi-metallic manganite LSMO contacting Bi2223. Below the Bi2223 superconducting transition temperature, bulk resistive losses in the nanostructures are determined by the current flowing through ferromagnetic LSMO nanoparticles that cover Bi2223 microgranules. As temperature decreases, proximity-induced superconducting transition in the effectively 2D surface of LSMO nanoparticles covering Bi2223 microgranules reveals itself as the topological BKT-like superconducting transition in the bulk sample.

Keywords: superconductor-ferromagnet nanostructures, the Berezinskii–Kosterlitz–Thouless transition.

1. Introduction

Hybrid half-metal ferromagnet (hmF)–superconductor (SC) nano-hetero-structures can enable new intelligently tailored functionality. They have gained attention over the past few years as promising functional materials for superconducting spintronics [1–3]. Apart from the purpose of superconducting spintronics' functional materials, transport properties of SC:hmF nanocomposites have been attracted a fundamental interest themselves, as well. One of the distinctive features of SC:hmF nanocomposites is a superconducting proximity effect that determines their superconducting characteristics to be beyond the conventional chaotic two-components structures. In particular, for SC:hmF nanocomposites geometric contacts of SC and hmF particles and electrical (supercurrent) connectivity of individual particles are often not the same thing [4–8].

To date, a few works have been reported on the study of transport properties of SC with half-metallic magnetic nanoparticles composites. Unconventional double percolation transition is identified by Liu *et al.* [4] for a binary network composed of nanoparticles of MgB_2 superconductor and CrO_2 half-metallic ferromagnet. It was shown that the double percolation transition (superconductor–insulator–metal) is controlled by the components volume fractions and originates from the suppressed interface conduction and tunneling as well as a large geometric disparity between particles [4]. In Ref. 5, Acharya *et al*. prepared and studied $Bi_2Sr_2CaCu_2O_8$:$BiFeO_3$ nanocomposite with various weight percentage of superparamagnetic $BiFeO_3$ nanoparticles.

Measurements of the samples' resistive characteristics give a demonstration of two steps, T_{c1} and T_{c2}, during to transition to overall superconducting state. Such behavior has been attributed to a weak-link nature of a granular SC as the latter is composed of superconducting grains embedded in a non-superconducting host. Of the two superconducting transitions temperatures, the higher one, T_{c1}, marks the superconductivity in grains whereas the grain boundary remains normal, and the lower one, T_{c2}, emerges when the grain boundary becomes superconducting, too. Just recently, transport characteristics of the MgB_2:$La_{2/3}Sr_{1/3}MnO_3$ (LSMO) nanocomposite with a 3:1 volume content of the components have been studied [9]. The experiment showed that the temperature behavior of the resistance of bulk MgB_2:LSMO samples during the transition to the superconducting state is described by the Berezinskii–Kosterlitz–Thouless (BKT) model for 2D SC [10–12]. It was argued that the observed transport features are most likely due to presence in the system of two characteristic spatial scales: (i) significant difference between geometrical dimensions of the constituent components (micrometer-sized particles of *s*-wave SC MgB_2 and nano-sized particles hmF LSMO), and (ii) the coherence length of proximity induced *p*-wave triplet superconducting state of half-metal manganite LSMO contacting with MgB_2. Resistive losses in such nanostructures are due to the current flow through ferromagnetic LSMO nanogranules that cover MgB_2 microgranules. As temperature decreases, the superconducting BKT transition occurs in 2D LSMO curved surface layers.

Conventional BKT superconducting transition has topological nature and is associated with the vortex-antivortex (un-)binding [13]. At temperatures below T_{BKT}, the vortex-antivortex pairs composite a bound state; for $T > T_{BKT}$, the vortex proliferation takes place, and the system enters a Coulomb gas-type state. This BKT topological transition is general and was observed in many two-dimensional systems with O(2) symmetry, such as superfluid and superconducting films [14], two-dimensional spin systems [15, 16], etc. Although the BKT transition is a well-known phenomenon on planar surfaces, for curved spaces the situation is not so clear. The realization of a classical BKT transition in nominally three-dimensional systems has not an obvious case *a priori* [9, 17–19], as well.

In this report, we present the results of the experimental investigation and theoretical description of the transition to a superconducting state of random binary nanocomposites of *d*-wave cuprate SC $Bi_2Sr_2Ca_2Cu_3O_{10+x}$ (Bi2223) microparticles and hmF $La_{2/3}Sr_{1/3}MnO_3$ (LSMO) nanoparticles — Bi2223:LSMO nanocomposites. Namely, we designed and fabricated a few random nanocrystalline samples by combining different volume ratios of the hmF (LSMO) and SC (Bi2223) components. To better understand thermodynamics and proximity-induced superconducting transition in the bulk (3D) nanocomposite, we have studied SC:hmF nanocomposites with the volume content of manganite nanoparticles that does not break up the system's percolation transition to a superconducting state and investigated their transport characteristics. It was detected that the experimental current-voltage (*I-V*) characteristics of the bulk nanocomposite samples, with 4:1 volume content of the components, undergoing superconducting transitions are described by the BKT model for 2D superconductors. A physical model has been discussed that provides an explanation of the similarity between the observed temperature dependences of the 3D nanocomposites resistivity $R(T)$ and *I-V* behavior within the 2D system's paradigms. We argue that the observed unusually large value of the concentration threshold for high-T_c SC, Bi2223, detected for the realization of this topologically 2D phase transition is due to two different physical spatial scales involved into the nanocomposite's bulk superconducting transport properties formation. Namely, these are: (i) significant difference between geometrical dimensions of the SC and hmF constituent components and (ii) necessity of "additional" (triplet) superconducting state induced by the proximity effect in half-metallic manganite nanoparticles and appearance of related superconducting correlation length. This paper is a continuation of our recently published report, Ref. 20, dealing with specifics percolation transitions in Bi2223:LSMO 3D nanocomposites.

2. Samples and measurement techniques

Bulk nanocomposite samples have been composed of *d*-wave high-T_c SC Bi2223 ($Bi_2Sr_2Ca_2Cu_3O_{10+x}$) microparticles and hmF LSMO ($La_{2/3}Sr_{1/3}MnO_3$) nanoparticles. The Bi2223 microparticles with dimensions $d \simeq (5–10)\times1\times0.5$ μm^3 were chosen as the superconducting ingredient considering a few factors. First, compressed Bi2223 powder samples have a low resistivity $\rho = 4\cdot10^{-3}$ Ohm·cm and their temperature dependence have a well-pronounced metallic character. This indicates that the intergranular boundaries have a small effect on the conductivity of the microparticles bulk sample. Second, the high critical temperature of the superconducting transition enables the characteristics of the composite material of interest to be studied in a broad temperature range. Note, the superconducting correlation length ξ_S of Bi2223 is known to be highly anisotropic and to have the value $\xi_{ab}(0) \approx 8$ nm in the *ab*-plane and $\xi_c(0) \sim$ $\sim$ 3 nm along the *c*-axis (see, e.g., [21] and references therein). Since the dimensions of the granules are significantly larger than the superconducting correlation length, $d >> \xi_S$, the temperature of the superconducting transition, T_{c0}, of individual granules remains close to 110 K that of bulk Bi2223. Third, in contrast to MgB_2, Bi2223 is a *d*-wave SC. Thus in the Bi2223:LSMO nanocomposites, as theory predicts [22–24], a superconducting state as a mixture of *d*- and *p*-waves superconducting order parameters will be realized.

The ferromagnetic component was $La_{2/3}Sr_{1/3}MnO_{3-\delta}$ manganite whose Curie temperature is $T_C \simeq 320–360$ K.

The LSMO nanopowder was obtained by deposition technology based on the sol-gel method (see details in Refs. 25, 26). The phase composition and dimensions of particles (~20–30 nm) were determined using x-ray diffraction analysis and electron microscopy. The data obtained confirmed that the LSMO nanoparticles feature a single-phase composition and perovskite structure. Measurements of magnetization and NMR studies on nanoparticles obtained by this technology have shown that nanoparticles maintain magnetic and transport characteristics close to those of a single-crystal LSMO. That is, their ferromagnetic state is due to the double-exchange interaction between Mn^{3+}–Mn^{4+} ions and characterizes a spin-polarized (half-metallic) conductivity (for more details see Refs. 27, 28).

Bulk samples were produced using the standard cold-pressing technology. The initial components were mixed in alcohol in accordance with their volume fractions and dried. Plates $\simeq 10\times1\times0.1$ mm^3 in size were pressed from the obtained mixture at pressures up to 40–60 kbar. This pressure ensures good electrical coupling between the grains and high mechanical strength of the plates. The samples were annealed at T = 650 °C for about 30 min to saturate with oxygen, yet not sintered to prevent mutual diffusion and chemical reactions between the components. The current and voltage contacts were deposited on the plate as a thin layer of colloidal silver in an area of the assumed contact with subsequent crimping. The junction resistance of the contact sites was $R \approx 10^{-8}$ Ohm. The electrotransport characteristics were measured using a four-probe setup in a broad temperature range (4.2–300 K). The cryogenic cooling was done in a gaseous medium of helium.

An analysis of the nanocomposite structure shows that the Bi2223 granules are snugly embraced by the nanosized LSMO grains. This assumption is supported by measurements of the sample's density. Namely, the density of the Bi2223 plates produced under a pressure of 40–60 kbar was (72 ± 3) % of the Bi2223 single-crystal density. The density of the LSMO nanopowder compressed under the same pressure was a mere (68 ± 3) % of the single-crystal density. At the same time, the density of the Bi2223:LSMO (25 % LSMO) composite was (96 ± 3) % of the calculated "crystal" density. Such a high composite density indicates that the LSMO nanoparticles "spread" under high uniaxial pressure across the sample volume, filling pores surrounding large Bi2223 granules (see the schematic rendering of the nanocomposite in Fig. 1, insert). The equality of the resistances of different samples of the same composition and the linear dependence of the resistance on the length of the plate section, obtained using six potential contacts, were taken as a criterion of a uniform distribution of the components over the sample's volume.

Note, the current-voltage dependence for bulk composite materials may be uncontrollably distorted due to the Joule heating, this circumstance should be considered when measuring the composite samples' resistivity $R(T)$ and current-voltage (I-V) characteristics. In the range of measuring currents, I = 0.1–1 mA, the curves of the $R(T)$ transition coincided. To avoid uncontrollable thermal effects, the studies were doing with the measurement currents in the range of I = 50–100 μA that did not cause any changes to sample characteristics which are related to heat dissipation factors. We also used an external high-frequency (HF) voltage signal, ~ 100 MHz, to investigate the microwaves effect on the nanocomposite's transport characteristics. A high-frequency signal has been connected by a coaxial cable to the current contacts of the sample through a C = 100 pF capacitor. We assume that the external signal generates microwave currents that suppress phase coherence between weakly bound contacts in the composite, which leads to broadening of the superconducting transition and a decrease in the excess current of the I-V characteristics.

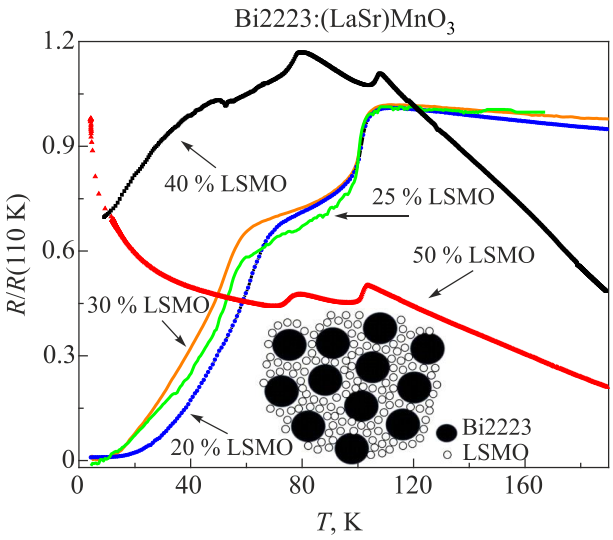

Fig. 1. (Color online) Temperature dependences of the nanocomposite's resistivity with the volume fraction, percentagewise, 20, 25, 30, 40, and 50 vol % of the LSMO. Inset: sketch of the nanocomposite structure. (Borrowed from Ref. 20).

3. Experimental results, effective medium approach

For a start-up reference, let us present the necessary results of the nanocomposites' transport characteristics with different vol % of LSMO; see Ref. 20. (Results of research of magnetoresonance properties of the Bi2223:LSMO nanocomposite are presented in Ref. 29.) As it follows from $R(T)$ nanocomposites' characteristics, Fig. 1, the superconductor-normal metal transition has been observed for the samples where the content of LSMO does not exceed 30 vol %. The experimental data presented in Fig. 1 point that the basic features of the bulk nanocomposite (critical transition temperature, percolation transition threshold, etc.) cannot be described in quantitative terms by standard percolation models [30–32] (for more details see Ref. 20). Below we concentrate attention on the transi-

tion features to a coherent superconducting state of the nanocomposites with 20 % volume fraction of the LSMO component.

It is well known that in the vicinity of the BKT transition to a superconducting state the resistance of thin 2D films is described by the expression (see, e.g., Ref. 13 and references therein):

$$R(T) = R_0 \exp\left\{-4\alpha\left[\frac{T_{c0} - T_{BKT}}{T - T_{BKT}}\right]^{1/2}\right\}. \qquad (1)$$

Here the parameter α is uniquely expressed in terms of the effective mass of the core of the fluctuating vortex and antivortex. It was shown [19, 33] that α is not an arbitrary constant of the order of unity but is causally related to the effective mass of the vortex core in a 2D superconductor. In most cases, when the two-dimensional nature of the film's superconducting transition is not in doubt, and especially for high-T_c cuprate SCs, the parameter α turned out to be limited by a rather narrow interval of $1 \lesssim \alpha \lesssim 1.5$ [19, 33].

Figure 2 (main panel) displays experimental temperature dependence of resistivity $R(T)$ of the 20 vol % of LSMO nanocomposite (black solid line) in a temperature range below T_{c0} of Bi2223. In addition to a steep fall of resistance at $T < T_{c0}$, see Fig. 1, there is a virtually parabolic dependence $R(T)$ in the temperature range ~ 30–60 K that is followed by a significant decrease in resistance. The most interesting observation is that the nanocomposite's resistance temperature behavior at $T < 55$ K is surprisingly well described by Eq. (1), red dashed curve in Fig. 2. As can be seen from the figure, the theoretical, Eq. (1), and experimental $R(T)$ dependences agree well in a broad temperature range of $\Delta T \approx$ 32–55 K, where the resistance R varies by 3 orders of magnitude. This $R(T)$ dependence

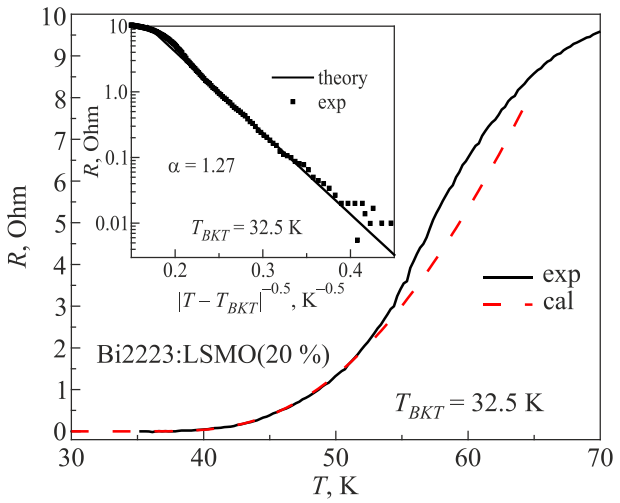

Fig. 2. (Color online) The nanocomposite's (20 % LSMO) resistance temperature dependence. Experimental, black solid curve, and theoretical, Eq. (1), red dashed curve, $R(T)$ behavior. Insert: an effective mass α of the vortex/antivortex core temperature dependence.

points that the 3D nanocomposite goes through the BKT-like transition similarly to a 2D system with the transition temperature $T_{BKT} \approx 32.5$ K and the parameter $\alpha \approx 1.27$ (see the inset in Fig. 2).

In the context of the genuine BKT transition broadening in inhomogeneous layered SCs, the temperature behavior of the *I-V* characteristic should correspond to the dependence $V \sim |I|^{a}(T)$, with the exponent $a(T_{BKT}) = 3$ and $a(T) \to 1$ above T_{BKT} [19, 33–36]. Figure 3 (main panel) displays a double logarithmic plot of the *I-V* characteristics of the sample with 20% LSMO at temperatures spanning the range $T_{BKT} \leq T < T_{c0}$. At $T = 52.5$ K the *I-V* curve is approximately linear, while at T_{BKT}, $V \sim I^3$. Experimental (points) temperature dependence of the parameter $a(T)$ in $V \sim |I|^{a}(T)$ dependence is summarized in the inset. The choice of T_{BKT} which provides the best fit to the resistance theory [34, 35] also corresponds to the value at which the *I-V* curves have an exponent $a(T_{BKT}) \approx 3$. We observe that the experimental *I-V* characteristics of bulk samples of nanocomposites with a volumetric content of 4:1 components are well described by the BKT model for 2D superconductors undergoing a superconducting transition [19, 33–36].

In the light of these observations, it is naturally to suggest that the sample's resistivity distinctive features are determined by an inhomogeneous spatial distribution of the local superconducting grains coupled by Josephson currents. To further test the validity of the experimental data interpretation, we analyze the effect of external microwave radiation on the nanocomposite's transport characteristics. Figure 4 shows the effect of the HF irradiation on resistive transitions in the temperature range $T < T_{c0}$ in the nanocomposites Bi2223:20% LSMO and in compacted Bi2223

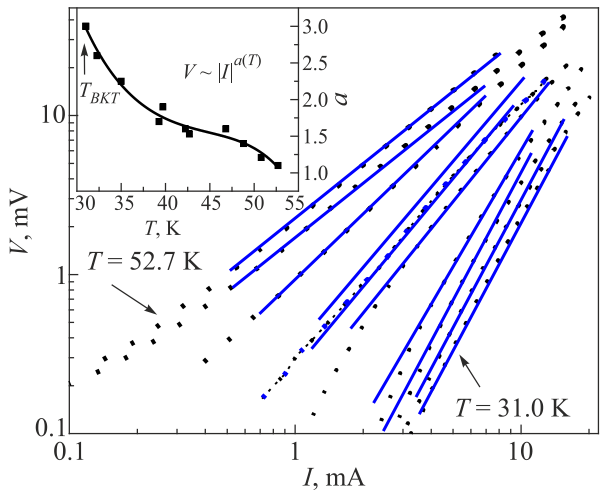

Fig. 3. (Color online) Logarithmic plot of the *I-V* characteristics of the sample 20 vol % LSMO at temperatures spanning the range $T_{BKT} \leq T < T_{c0}$ (T = 31.0, 32.3, 39.3, 39.7, 42.3, 42.7, 46.8, 48.8, 50.8, and 52.7 K); dotted lines are experiment, blue solid lines are theory. Insert: Experimental (points) and quadratic approximation (solid line) temperature dependence of the parameter $a(T)$, $V \sim |I|^{a}(T)$.

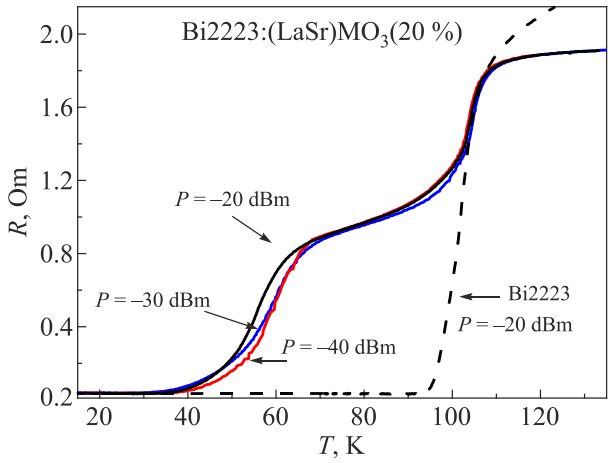

Fig. 4. (Color online) Effect of the HF voltage signal ~100 MHz on the resistive transition of the Bi2223 sample and nanocomposites with 20 % of LSMO.

sample. As it is shown in Fig. 4, the HF signal applied to the compacted Bi2223 sample does not cause noticeable changes in the $R(T)$ dependence. At the same time, we notice from Fig. 4 that if the nanocomposite is a subject of the HF voltage signal, a tail with upward curvature changes demonstrating increasing resistance. This is typical for the fluctuation resistivity near the T_{BKT} transition [36]: the resistive tail can be attributed to inhomogeneous spatial distribution of the local superfluid caused by intrinsic inhomogeneous density distribution (superconducting granules, in our case, see Sec. 4) in the systems.

The changes in the *I-V* characteristics of the 20% LSMO nanocomposite's superconducting state under the HF radiation are shown in Fig. 5. At small amplitudes of the time dependent voltage signal, an increase in the resistance and a decrease in the excess current indicates that weak couplings (Josephson contacts) are suppressed in the –Bi2223–LSMO–Bi2223– chains (see Sec. 4). Thus, the

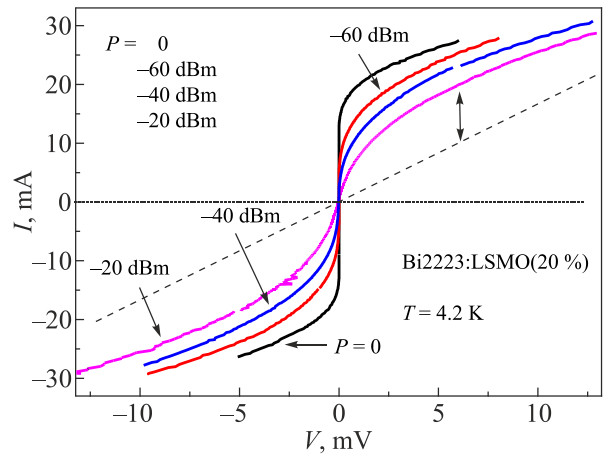

Fig. 5. (Color online) Effect of the HF voltage signal ~100 MHz on the *I-V* characteristics of the nanocomposite with 20 vol % of LSMO.

transport characteristics of the 3D nanocomposite are extremely sensitive to the external microwave signal.

The main physical message of the experimental data in Figs. 2–5 is as follows: the 3D nanocomposite bulk superconducting transition reproduces the main feature of the BKT superconducting transition in 2D systems. Correspondence of the key features of the 2D BKT transition with the experimental data for the 3D nanocomposite means the realization of effective 2D (not, naturally, flat) surfaces undergoing the transition to a superconducting state within the BKT scenario in our 3D inhomogeneous samples.

4. Discussion

As has been discussed at length in the literature (see, for example, Refs. 13, 14, and references therein), the distinguishing feature of the 2D systems superconducting transition is that gas of superconducting fluctuations may exist in the form of spontaneously generated magnetic vortices at a temperature below the temperature T_{c0} of the bulk superconducting transition. The vortices are generated in pairs with opposite directions of ring currents (vortex–antivortex pairs), which annihilate after a finite time because of collisions. In a zero magnetic field, the number of vortices having opposite signs coincides and is determined by the dynamic equilibrium between their spontaneous generation and annihilation. The wave-function phase changes because of going around an immobile vortex by 2π; therefore, the free motion of vortices results in fluctuations of the phase. If the amplitude of the fluctuations is large enough, the coherence of the superconducting state disappears, yet, the order parameter modulus $\Delta(\mathbf{r})$ remains non-zero in most of the sample volume and vanishes only near the vortex cores.

If the temperature decreases, the BKT transition occurs at a temperature T_{BKT} ($< T_{c0}$), where vortex pairs are no longer generated, vortex density sharply decreases to become exponentially small, and dissipation becomes exponentially small, as well. Therefore, in the temperature range $T_{BKT} < T < T_{c0}$, Cooper pairs coexist in 2D superconductors with vortices. Dissipation decreases due to the presence of Cooper pairs but does not vanish. In samples with defects, the BKT transition broadens due to an internal inhomogeneous spatial distribution of the superfluid [19].

If we deal with a 2D system consisting of superconducting granules embedded into a normal (non-magnetic) metal, the superconducting state is destroyed by another mechanism (see [37] and the references therein). In this case, the transition to the resistive state occurs due to the loss of phase coherence in the system with a finite order-parameter modulus $\Delta(\mathbf{r})$ in individual superconducting granules. This implies that the bulk system is in the dissipative state, while individual granules stay in the superconducting state. In this case, the charge may be transferred from one granule to another via two channels $j_{\text{tot}} = j_S + j_N$: by the Josephson current j_S and by a current of uncorrelated electrons j_N. If the charge is transferred by the Josephson current of Cooper

pairs, the phases of the order parameter between granules participating in the current transfer are correlated, and a macroscopic superconducting state is established between them. However, the Josephson currents can be suppressed by fluctuations due to a large normal resistivity between granules or by external factors, such as the HF radiation, [37, 38]. In this case, the charge is transferred between the granules due to single-particle excitations, $j_{\rm tot} \to j_N = eN_e$, the concentration of which N_e, is exponentially small in the granules due to their superconducting state: $N_e \propto \exp\left(-\Delta(\mathbf{r})/T\right)$ (e is the electron charge). At low temperatures, the microwaves can induce large suppression of the supercurrent and the resistive state with a non-zero equilibrium density of Cooper pairs is realized in the system [38, 39]. This is manifested experimentally by the diminution of an excess current under the microwave-field effect in the *I-V* characteristics of the sample.

In layered superconductor/normal metal proximity coupled structures, distinctive features of the BKT transitions were studied, as well. Particularly, in proximity coupled Pb–Sn film contacts in the temperature range $T_{c0}(\mathrm{Sn}) \approx 3.75$ K $< T <$ $< T_{c0}(\mathrm{Pb}) \approx 7.3$ K the authors of Ref. 36 observed a resistive transition to the superconducting state that reproduces the main features of the BKT transition. In the same temperature range, nonlinear *I-V* characteristics were observed that had been predicted in Refs. 34 and 35 for the case of topological ordering of vortices in 2D superconductors. The layered proximity SC/hmF structures have been actively studied using both experimental and theoretical approaches (see, e.g., [24, 40–46] and references therein).

For a bulk composite with roughly the same geometrical size of components, the conventional lattice percolation model [30–32] predicts $f_c = 0.16 \pm 0.02$ for the percolation threshold of the volume fraction, f, of a conducting component. It is well established, when grains of the superconducting material, d, are large enough, $d >> \xi_S$, their basic intra-granular characteristics (critical temperature, superconducting gap, etc.) are not affected by the proximity of the non-superconducting component and remain close to the bulk value of a quantity. Thus, according to the lattice percolation model, for the nanocomposite systems under consideration with large grains of the superconducting material and the volume fraction above the percolation threshold f_c, the bulk superconducting transition temperature T_c should not be strongly dependent on the contents variation. However, as it is seen in Fig. 1, even for the sample with the volume fraction about three times larger than the conventional percolation model predicts, there is no transition into a superconducting state. Thus, the predictions based on the conventional percolation models fail for the Bi2223:LSMO nanocomposites most probably due to two factors: (i) essential difference in the components' geometrical size and, as a necessary condition, (ii) transition the hmF nanoparticles into a superconducting state due to superconducting proximity effect.

As is known, below the superconducting transition, an indirect (due to the proximity effect) coupling between constituent components emerges. In SC/hmF heterostructures a long-range proximity effect will be realized effectively, and a triplet component of anomalous correlations should be taken into consideration [24, 40–47]. In previous works, anomalous superconductivity has been indeed detected in SC/hmF nanostructures [48, 49] and in SC/hmF junctions [50–53]. It was argued that at low-temperatures, manganites are thermodynamically close to a superconducting state with a triplet p-wave even frequency pairing [48–52]. Being proximity coupled to a singlet SC, the $m = 0$ triplet wave-function component is coupled in the manganite via the boundary condition to the singlet pairing amplitude in the SC partner. At the same time, the spin-active boundary leads to coupling of the $m = 0$ triplet component with an equal-spin, $m = 1$, pairing amplitude in manganite. These couplings yield phase coherency of both the $m = 0$ and equal-spin $m = 1$ triplet Cooper pairs in the hmF manganite. Dependence of the scale of superconducting correlations on the intrinsic magnetic field inhomogeneity is a feature of the proximity effect in mesoscopic hmF/SC structures [22, 23, 47].

Thus, in the case of the nanocomposite under consideration, the proximity effect possesses a few specific peculiarities. First, because the contacts between Bi2223 grains in the bulk are through the half-metallic LSMO nanograins, this causes significant broadening of the nanocomposite transition to a superconducting state. Second, for high-T_c SCs with d-wave Cooper pairs symmetry [22], theory predicts, and experiment provides evidence that in proximity coupled d-wave SC/ferromagnet structures an unconventional (spin-triplet) superconducting state can be generated. This also means that in the nanocomposite a new geometrical length has been generated which characterizes an unconventional superconducting state (a mixture of d-wave singlet and p-wave triplet Cooper pairs) in proximity-coupled regions. Characteristic coherence length of triplet correlations $\xi_F = (D_F/2\pi T)^{1/2}$ can be as large as ~ 100 nm at low temperatures (here D_F is the diffusivity of the ferromagnet metal, $h = k_B = 1$)

Under these specific conditions, the nanocomposite's transition to a superconducting state, most probably, is followed the next "evolution scenario". The onset of superconductivity occurs independently in each Bi2223 microgranules at the temperature of superconducting condensate formation in the bulk Bi2223. The magnetic fluxes are caused by the manganite nanoparticles' magnetization and at temperatures $T < T_{c0} < T_C$(LSMO) the magnetic fluxes are confined to the manganite nanoparticles [54]. That is, in the temperature range $T_{BKT} < T < T_{c0}$ a resistive state emerged in the nanocomposite is featured by a nonzero equilibrium concentration of Cooper pairs in the Bi2223 microparticles and frozen magnetic vortices/fluxes created by the LSMO nanoparticles. I.e., the 3D structure formed in the system

consists of the superconducting granules covered by the ferromagnetic nanoparticles: –hmF–SC–hmF–SC–"brickwork" 3D structure. If the temperature decreases further, BKT-like superconducting transition is realized in the bulk Bi2223:LSMO nanocomposite due to the emergence of an effective 2D percolation cluster of a specific superconducting state. Namely, the 2D supercurrent percolation is fulfilled through hmF nanoparticles layer following the "brickwork" scheme. Due to the proximity effect at magnetically inhomogeneous Bi2223–LSMO interfaces, the superconducting state of the percolation layer is a mixture of *d*-wave singlet and *p*-wave triplet Cooper pairs.

5. Conclusion

The features of the superconducting transition in chaotic two-component nanostructures, nanocomposites consisting of *d*-wave *SC* $Bi_2Sr_2Ca_2Cu_3O_{10+x}$ microparticles, and nanoparticles of half-metallic $La_{2/3}Sr_{1/3}MnO_3$ ferromagnets, are studied. The nanocomposite samples with 4:1 volume content of the components undergoing bulk superconducting transitions are satisfactory described by the Berezinskii–Kosterlitz–Thouless model for two-dimensional superconductors. The observed 2D topological transport characteristics of the nanocomposites are due to two physical spatial scales typical for this type of systems: (i) significant difference between geometrical dimensions of the constituent components (micro-meter sized Bi2223 and nano-meter sized LSMO particles) and (ii) appearance of related superconducting correlation length of "additional" (triplet) superconducting state induced by the proximity effect in half-metallic manganite nanoparticles. The reduction of effective dimensionality for superconducting correlations has resulted in the resistive losses determined by the current flowing through the ferromagnetic LSMO nanogranules covering the $Bi_2Sr_2Ca_2Cu_3O_{10+x}$ microgranules. As the temperature decreases, the BKT-like transition occurs in effectively 2D LSMO surface that undergoes to a superconducting state due to the proximity effect. Apart from its fundamental interest, the transport properties of high-T_c SC:hmF nanocomposites are relevant for superconducting spintronics as potential functional materials. With continuous advance in manufacturing spintronic devices, the results obtained can be useful to better understanding of thermodynamics and the phase transition of this type of nano-hetero-structures — a crucial factor in design of corresponding devices.

Acknowledgments

The authors are grateful to I. Danilenko and O. Gorban' for the fabrication of manganite nanoparticles. We also thank M. Belogolovskii for reading the manuscript and fruitful discussions. The work is supported by the Targeted program fundamental research of the NAS of Ukraine "Promising basic research and innovative developments nanomaterials and nanotechnologies for industry, health and agriculture" (Project No. 17/21-H).

1. Y. C. Tao and J. G. Hu, *J. Appl. Phys.* **107**, 041101 (2010).
2. S. Anders, M. G. Blamire, F.-I. Buchholz, D.-G. Crété, R. Cristiano, P. Febvre, L. Fritzsch, A. Herr, E. Il'ichev, J. Kohlmann, J. Kunert, H.-G. Meyer, J. Niemeyer, T. Ortlepp, H. Rogalla, T. Schurig, M. Siegel, R. Stolz, E. Tarte, H. J. M. ter Brake, H. Toepferm, J.-C. Villegier, A. M. Zagoskin, and A. B. Zorin, *Physica C* **470**, 2079 (2010).
3. J. Linder and J. M. A. Robinson, *Nat. Phys.* **11**, 307 (2015).
4. X. Liu, R. P. Panguluri, Z.-F. Huang, and B. Nadgorny, *Phys. Rev. Lett.* **104**, 035701 (2010).
5. S. Acharya, A. K. Biswal, J. Ray, and P. N. Vishwakarma, *J. Appl. Phys.* **112**, 053916 (2012).
6. Y. M. Strelniker, A. Frydman, and S. Havlin, *Phys. Rev. B* **76**, 224528 (2007).
7. I. Sternfeld, V. Shelukhin, A. Tsukernik, M. Karpovski, A. Gerber, and A. Palevski, *Phys. Rev. B* **71**, 064515 (2005).
8. L. Ruiz-Valdepeñas, M. Vélez, F. Valdés-Bango, L. M. Álvarez-Prado, J. I. Martín, E. Navarro, J. M. Alameda, and J. L. Vicent, *New J. Phys.* **15**, 103025 (2013).
9. A. I. D'yachenko, V. Yu. Tarenkov, and V. N. Krivoruchko, *Fiz. Nizk. Temp.* **45**, 1360 (2019) [*Low Temp. Phys.* **45**, 1156 (2019)].
10. V. L. Berezinsky, *JETP* **59**, 907 (1971) [*Sov. Phys. JETP* **32**, 493 (1971)].
11. J. M. Kosterlitz and D. J. Thouless, *J. Phys. C* **6**, 1181 (1973).
12. J. M. Kosterlitz, *J. Phys. C* **7**, 1046 (1974).
13. G. Blatter, M. V. Feigel'man, V. B. Geshkenbein, A. I. Larkin, and V. M. Vinokur, *Rev. Mod. Phys.* **66**, 1125 (1994).
14. A. M. Goldman, *The Berezinskii–Kosterlitz–Thouless Transition in Superconductors*, in: *40 Years of Berezinskii-Kosterlitz-Thouless Theory*, J. V. José (ed.), World Scientific, Singapore (2013), p. 135.
15. B. V. Costa and A. B. Lima, *J. Magn. Magn. Mater.* **324**, 1999 (2012).
16. U. Tutsch, B. Wolf, S. Wessel, L. Postulka, Y. Tsui, H. O. Jeschke, I. Opahle, T. Saha-Dasgupta, R. Valentí, A. Brühl, K. Remović-Langer, T. Kretz, H.-W. Lerner, M. Wagner, and M. Lang, *Nat. Commun.* **5**, 5169 (2014).
17. P. Minnhagen, *Rev. Mod. Phys.* **59**, 1001 (1987).
18. A. Ashoka, K. S. Bhagyashree, and S. V. Bhat, *Phys. Rev. B* **102**, 024429 (2020).
19. L. Benfatto, C. Castellani, and T. Giamarchi, *Phys. Rev. B* **80**, 214506 (2009).
20. V. N. Krivoruchko and V. Yu. Tarenkov, *Fiz. Nizk. Temp.* **45**, 555 (2019) [*Low Temp. Phys.* **45**, 476 (2019)].
21. G. Wang, M. Raine, and D. P. Hampshire, *Supercond. Sci. Technol.* **31**, 024001 (2018).
22. M. Eschrig and T. Löfwander, *Nature Phys.* **4**, 138 (2008).
23. M. Eschrig, *Phys. Today* **64**, 43 (2011).
24. A. Frano, S. Blanco-Canosa, E. Schierle, Y. Lu, M. Wu, M. M. Bluschke, M. Minola, G. Christiani, H. U. Habermeier, G. Logvenov, Y. Wang, P. A. van Aken, E. Benckiser, E. Weschke, M. Le Tacon, and B. Keimer, *Nature Mater.* **15**, 831 (2016).

25. M. M. Savosta, V. N. Krivoruchko, I. A. Danielenko, V. Y. Tarenkov, T. E. Konstantinova, A. V. Borodin, and V. N. Varyukhin, *Phys. Rev. B* **69**, 024413 (2004).
26. V. Krivoruchko, T. Konstantinova, A. Mazur, A. Prokhorov, and V. Varyukhin, *J. Magn. Magn. Mater.* **300**, E122 (2006).
27. A. S. Mazur, V. N. Krivoruchko, and I. A. Danilenko, *Fiz. Nizk. Temp.* **33**, 1227 (2007) [*Low Temp. Phys.* **33**, 931 (2007)].
28. A. N. Ulyanov, D. S. Yang, A. S. Mazur, V. N. Krivoruchko, G. G. Levchenko, I. A. Danilenko, and T. E. Konstantinova, *J. Appl. Phys.* **109**, 123928 (2011).
29. T. V. Kalmykova, S. Yu. Polevoy, S. V. Nedukh, S. I. Tarapov, and V. Yu. Tarenkov, *Funct. Mater.* **21**, 302 (2014).
30. S. Kirkpartrick, *Rev. Mod. Phys.* **45**, 574 (1973).
31. A. Bunde and W. Dieterich, *J. Electroceram.* **5**, 81 (2000).
32. I. Balberg, *J. Phys. D* **42**, 064003 (2009).
33. L. Benfatto, C. Castellani, and T. Giamarchi, *Phys. Rev. B* **77**, 100506(R) (2008).
34. B. I. Halperin and D. R. Nelson, *J. Low Temp. Phys.* **36**, 599 (1979).
35. S. Doniach and B. A. Huberman, *Phys. Rev. Lett.* **42**, 1169 (1979).
36. D. J. Resnick, J. C. Garland, J. T. Boyd, S. Shoemaker, and R. S. Newrock, *Phys. Rev. Lett.* **47**, 1542 (1981).
37. V. F. Gantmakher, *Fiz. Nizk. Temp.* **37**, 71 (2011) [*Low Temp. Phys.* **37**, 59 (2011)].
38. F. S. Bergeret, P. Virtanen, A. Ozaeta, T. T. Heikkilä, and J. C. Cuevas, *Phys. Rev. B* **84**, 054504 (2011).
39. A. V. Semenov, I. A. Devyatov, P. J. de Visser, and T. M. Klapwijk, *Phys. Rev. Lett.* **117**, 047002 (2016).
40. Z. P. Niu and D. Y. Xing, *Phys. Rev. Lett.* **98**, 057005 (2007).
41. T. Hu, H. Xiao, C. Visani, Z. Sefrioui, J. Santamaria, and C. C. Almasan, *Phys. Rev. B* **80**, 060506(R) (2009).
42. K. Dybko, K. Werner-Malento, P. Aleshkevych, M. Wojcik, M. Sawicki, and P. Przyslupski, *Phys. Rev. B* **80**, 144504 (2009).
43. Yo. Kalcheim, T. Kirzhner, G. Koren, and O. Millo, *Phys. Rev. B* **83**, 064510 (2011).
44. W. Wang, D. F. Shao, R. C. Xiao, W. J. Lu, and H. Y. Wu, *J. Supercond. Nov. Magn.* **29**, 1741 (2016).
45. F. S. Bergeret, A. F. Volkov, and K. B. Efetov, *Phys. Rev. Lett.* **86**, 4096 (2001).
46. A. Kadigrobov, R. I. Shekhter, and M. L. Jonson, *Europhys. Lett.* **54**, 394 (2001).
47. M. Eschrig, J. Kopu, J. C. Cuevas, and G. L. Schön, *Phys. Rev. Lett.* **90**, 137003 (2003).
48. V. N. Krivoruchko and V. Y. Tarenkov, *Phys. Rev. B* **86**, 104502 (2012).
49. V. N. Krivoruchko, A. I. D'yachenko, and V. Yu. Tarenkov, *Fiz. Nizk. Temp.* **40**, 1147 (2014) [*Low Temp. Phys.* **40**, 895 (2014)].
50. V. N. Krivoruchko and V. Y. Tarenkov, *Phys. Rev. B* **75**, 214508 (2007).
51. V. N. Krivoruchko and V. Yu. Tarenkov, *Phys. Rev. B* **78** 054522 (2008).
52. C. Visani, Z. Sefrioui, J. Tornos, C. Leon, J. Briatico, M. Bibes, A. Barthélémy, J. Santamaría, and J. E. Villegas, *Nature Phys.* **8**, 539 (2012).
53. A. Cerreta, R. Gaina, L. Nuccio, I. Marozau, K. Sen, R. A. de Prada, S. Sarkar, and C. Bernhard, *Europhys. Lett.* **129**, 37002 (2020).
54. M. V. Milošević and F. M. Peeters, *J. Low Temp. Phys.* **139**, 257 (2005).

Двовимірний топологічний фазовий перехід Березинського–Костерліца–Таулесса у тривимірних нанокомпозитах $Bi_2Sr_2Ca_2Cu_3O_{10+x}$:(La,Sr)MnO_3

A. I. D'yachenko, V. N. Krivoruchko, V. Yu. Tarenkov

Досліджено електротранспортні властивості випадкових бінарних мереж, що складаються з мікрочастинок високотемпературного надпровідника $Bi_2Sr_2Ca_2Cu_3O_{10+x}$ (Bi2223) і наночастинок напівметалевого феромагнетика $La_{2/3}Sr_{1/3}MnO_3$ (LSMO). Експериментальні вольт-амперні характеристики об'ємних зразків нанокомпозиту з об'ємним вмістом компонентів 4:1 при переході в надпровідний стан добре описуються моделлю Березинського–Костерліца–Таулесса (БКТ) для двовимірних (2D) надпровідників. Спостережена 2D-подібна поведінка тривимірних транспортних властивостей нанокомпозиту, найбільш імовірно, обумовлена двома різними фізичними просторовими масштабами, які формують властивості нанокомпозиту: значна різниця між геометричними розмірами складових компонентів та поява триплетного надпровідного стану індукованого ефектом близькості в напівметалевому манганіті LSMO, що контактує з Bi2223. Нижче температури надпровідного переходу Bi2223 об'ємні резистивні втрати в наноструктурі визначаються струмом, що протікає через феромагнітні наночастинки LSMO, які покривають мікрогранули Bi2223. При зниженні температури індукований близькістю надпровідний перехід реалізується на 2D-поверхні наночастинок LSMO, що покривають мікрогранули Bi2223, та проявляється як топологічний БКТ-подібний надпровідний перехід в масивному зразку.

Ключові слова: надпровідниково-феромагнітні наноструктури, перехід Березинського–Костерліца–Таулесса.